Ratiometric Nanothermometer Based on an Emissive Ln^{3+}-Organic Framework

Amandine Cadiau,[†,§] Carlos D. S. Brites,[‡,§] Pedro M. F. J. Costa,[†,§] Rute A. S. Ferreira,[‡,§] João Rocha,[†,§,*] and Luís D. Carlos[‡,§,*]

[†]Department of Chemistry, [‡]Department of Physics, and [§]CICECO, University of Aveiro, 3810-193 Aveiro, Portugal

ABSTRACT Luminescent thermometers working at the nanoscale with high spatial resolution, where the conventional methods are ineffective, have emerged over the last couple of years as a very active field of research. Lanthanide-based materials are among the most versatile thermal probes used in luminescent nanothermometers. Here, nanorods of metal organic framework $Tb_{0.99}Eu_{0.01}(BDC)_{1.5}(H_2O)_2$ (BDC = 1-4-benzendicarboxylate) have been prepared by the reverse microemulsion technique and characterized and their photoluminescence properties studied from room temperature to 318 K. Aqueous suspensions of these nanoparticles display an excellent performance as ratiometric luminescent nanothermometers in the physiological temperature (300−320 K) range.

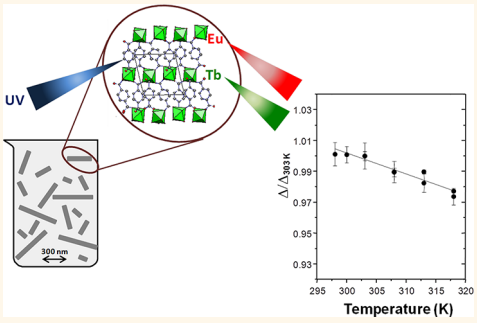

KEYWORDS: lanthanides · luminescence · metal−organic framework · nanothermometer · ratiometric

Luminescent thermometers working at the nanoscale with high-spatial resolution have emerged over the past few years, making this a very active field of research with potential applications in nanotechnology and nanomedicine.[1−3] Lanthanide (Ln)-based materials are among the most versatile thermal probes used in luminescent nanothermometers.[4−7] Ratiometric (or self-referencing) intensity measurements avoid the drawbacks of the experiments based on a single-transition intensity (such as the variation dependence of the sensor's concentration, material's inhomogeneities and optoelectronic drifts of the excitation source and detectors) as they are very reliable for precise-temperature sensing. Examples of ratiometric Ln-based nanothermometers include (Er^{3+}, Yb^{3+})-,[2,7−9] (Tm^{3+}, Yb^{3+})-,[10] Er^{3+}-[11] and Nd^{3+}-based[12] up-conversion nanoparticles (NPs), (Eu^{3+}, Tb^{3+}) mixed metal−organic framework (MOF),[13] a siloxane hybrid co-doped with a Eu^{3+} complex and an organic dye,[5] and siloxane hybrid magnetic NPs[4,14] and hybrid films[15] doped with Eu^{3+} and Tb^{3+} tris(β-diketonate) chelates.

MOFs are very promising multifunctional luminescent materials largely due to the presence of metal ions or clusters and organic linkers, providing a wealth of opportunities for engineering properties.[16−18] Moreover, the guest molecules they host may further assist in tuning the luminescence properties. A number of studies report the use of MOF NPs in sensing, biomedical imaging and drug delivery.[19−22] Applications of luminescent MOFs in chemical sensing and light-emitting devices are also well documented.[23−30] In contrast, little work is available on the preparation of NPs of Ln^{3+}-MOFs which, however, present considerable potential as nanoplatforms for biological and biomedical applications.[31,32]

Recently, Cui *et al.* reported the first ratiometric luminescent MOF thermometer, $(Eu_{0.0069}Tb_{0.9931})_2(DMBDC)_3(H_2O)_4 \cdot DMF \cdot H_2O$ (DMBDC = 2,5-dimethoxy-1,4-benzenedicarboxylate), based on the emissions of Tb^{3+} at 545 nm and Eu^{3+} at 613 nm.[13] This material, however, exhibits a linear response only in the range 50−200 K (thus, not covering the physiological range, ~300−320 K) and consists of micrometer-size particles. Building upon this work, here we propose a $Tb_{0.99}Eu_{0.01}(BDC)_{1.5}(H_2O)_2$ (BDC = 1-4-benzendicarboxylate) MOF (**1**) self-referencing, ratiometric, luminescent nanothermometer as a platform for

* Address correspondence to rocha@ua.pt, lcarlos@ua.pt.

Received for review May 23, 2013 and accepted July 19, 2013.

Published online July 19, 2013
10.1021/nn402608w

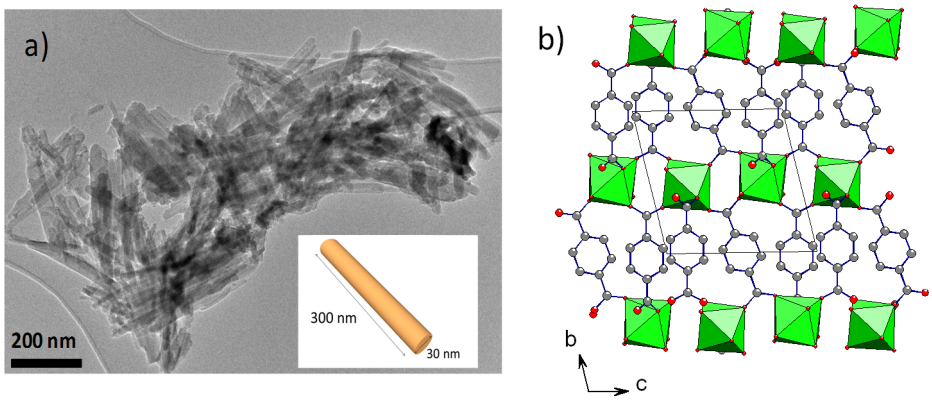

Figure 1. (a) TEM image of $Tb_{0.99}Eu_{0.01}(BDC)_{1.5}(H_2O)_2$ (1) nanorods; (b) crystal structure of 1 viewed along the *a*-axis (Tb/Eu, green polyhedra; C, gray; O, red; H atoms are omitted for clarity).

nanomedicine applications. Because of (i) their excellent sensing performance in the range of physiological temperatures in the form of an aqueous suspension, and (ii) the possibility of further co-doping with Gd^{3+}, these particles present a considerable potential for applications of biological interest, particularly in multimodal (thermal, optical and magnetic resonance) imaging.

RESULTS AND DISCUSSION

Nanorods of **1** were prepared by a reverse microemulsion method.[31,32] Briefly, two CTAB/1-hexanol/isooctane/water microemulsions with $W = 5$ (W is defined as water-to-surfactant molar ratio; CTAB = cetylmethylammonium bromide) containing Na_2BDC and $TbCl_3/EuCl_3$ (molar ratio 99:1) were combined and stirred vigorously for 2.5 h. The NPs of **1** were isolated by centrifugation and washed with ethanol. As shown by TEM (Figure 1a), they consist of crystalline nanorods with average length and diameter of 300 and 30 nm, respectively.

Powder X-ray diffraction confirms that **1** is crystalline and corresponds to the bulk phase $Tb(BDC)_{1.5}(H_2O)_2$ (Figure S1, Supporting Information), first reported in Reineke *et al.*[33] The three-dimensional structure of $Tb_{0.99}Eu_{0.01}(BDC)_{1.5}(H_2O)_2$ is built up from terephthalate ligands and isolated Ln^{3+} polyhedra (Figure 1b). Each Ln^{3+} ion is eight-coordinated to six bridging carboxylate groups from six terephthalate ligands, with two water molecules completing the coordination sphere. The BDC ligand bridges a total of four Ln^{3+} centers. The overall structure may be described as the stacking of alternating inorganic and organic layers along the *b*-axis.

To assess the potential of **1** to be used as a nanothermometer, the temperature dependence of its emission was investigated. Both solid particles and a salt-solution suspension were studied. The temperature was cycled three times in the 290−320 K range and the emission and excitation spectra were recorded (Figure 2 and Figure S2, Supporting Information). The spectra of the solid particles and suspensions, before and after temperature cycling, are exactly the same, thus excluding any structural change induced by the temperature variation (Figure S3, Supporting Information); this conclusion is supported by powder XRD (Figure S1, Supporting Information). We note, in passing, that issue of the stability of **1** in various solvents was previously addressed by Chen *et al.*[20] Upon excitation at 320 nm, **1** exhibits the characteristic $^5D_4 \rightarrow {}^7F_{6-4}$ (Tb^{3+}) and $^5D_0 \rightarrow {}^7F_{0-4}$ (Eu^{3+}) transitions. When we compare the excitation spectra of **1** (monitored at 698 nm, $Eu^{3+}{}^5D_0 \rightarrow {}^7F_4$, to avoid overlap with the Tb^{3+} emission lines) and $Tb(BDC)_{1.5}(H_2O)_2$ (monitored at 545 nm, $Tb^{3+}{}^5D_4 \rightarrow {}^7F_5$), the presence of the $^7F_6 \rightarrow {}^5G_{6,5}$, $^5L_{10}$, $^5D_{3,4}$, Tb^{3+} lines in the former spectrum is evident, indicating a Tb^{3+}-to-Eu^{3+} energy-transfer process (Figure S2a, Supporting Information).

Further evidence for Tb^{3+}-to-Eu^{3+} energy transfer is forthcoming from the $^5D_4$ and $^5D_0$ emission-decay curves. The $^5D_4$ decay curves of **1** excited at 377 nm (Tb^{3+} level) and within the ligand (270 and 320 nm) display a single-exponential behavior (Figure S4 and Table S1, Supporting Information). The dependence of the lifetimes on the excitation wavelength is in accord with a model proposed recently to describe the dependence of the lifetime on the excitation energy in the presence of intramolecular-energy transfer.[34] Irrespective of the excitation wavelength, the lifetime values are always smaller than the values measured for $Tb(BDC)_{1.5}(H_2O)_2$ (Figure S5 and Table S2, Supporting Information). Moreover, the $^5D_0$ decay curves under excitation via the excited-ligand levels exhibit a rising part (between 10^{-5} and 10^{-3} s, Figures S6 and S7, Supporting Information) before decaying, indicating that some source is feeding the $^5D_0$ level. The fitted rise time and the $^5D_4$ intrinsic lifetime are similar, supporting nonradiative Tb^{3+}-to-Eu^{3+} energy transfer. A simple definition of the Tb^{3+}-to-Eu^{3+} energy-transfer probability in terms of the $^5D_4$ donor lifetime in the presence (τ) and absence (τ_0) of the Eu^{3+} acceptors is[35,36]

$$P_{Tb \rightarrow Eu} = \frac{1}{\tau} - \frac{1}{\tau_0} \quad (1)$$

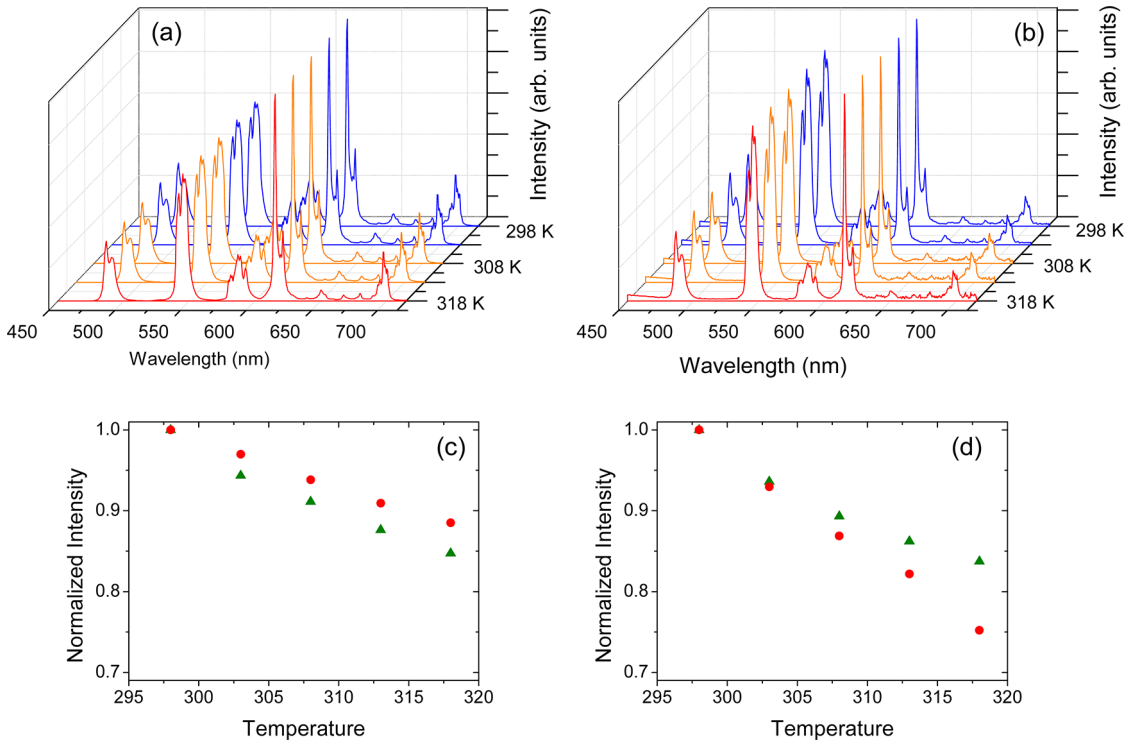

Figure 2. Emission spectra of 1 in (a) the solid state and (b) aqueous suspension (0.36 g·L^{-1}) in the physiologic-temperature range excited at 320 nm. Temperature dependence of the normalized-integrated intensity of the $^5D_4 \rightarrow {}^7F_5$ (Tb^{3+}, green) and $^5D_0 \rightarrow {}^7F_2$ (Eu^{3+}, red) transitions in (c) the solid state and (d) aqueous suspension.

whereas the corresponding energy-transfer efficiency is[35,36]

$$E_{Tb \rightarrow Eu} = 1 - \frac{\tau}{\tau_0} \quad (2)$$

For 320 nm, $P_{Tb \rightarrow Eu}$ and $E_{Tb \rightarrow Eu}$ are 0.37 $\times$ 10^3 s^{-1} and 23.1%, respectively (Cui *et al.*[13] reported a $E_{Tb \rightarrow Eu}$ value of *ca.* 40%). The maximum emission-quantum yields of **1** in the form of solid NPs and in suspension are 0.39 $\pm$ 0.04 and 0.23 $\pm$ 0.02 (excitation at 320 nm), respectively. There are very few reports of MOFs emission-quantum yields,[17] including the following for NPs: 0.07 for $Eu(BDC)_{1.5}(H_2O)_2$, 0.26, for $Tb(BDC)_{1.5}(H_2O)_2$,[37] and 0.39 for $([(Eu,Tb)(C_6H_8O_4)_3(H_2O)_2]\cdot(C_{10}H_8N_2)$.[38]

The luminescent intensity of Tb^{3+} and Eu^{3+} in **1** decreases gradually as the temperature increases between 290 and 320 K (Figure 2a) as expected from the thermal activation of nonradiative-decay pathways. The temperature-dependence of the emission spectra is evident from the integrated areas of the $^5D_0 \rightarrow {}^7F_2$ (Eu^{3+}, I_{Eu}) and $^5D_4 \rightarrow {}^7F_5$ (Tb^{3+}, I_{Tb}) transitions (Figure 2c). As the $^5D_4 \rightarrow {}^7F_5$ transition is almost insensitive to the Tb^{3+} local environment, due to its magnetic dipole character, the decrease with temperature of its integrated area is similar for powders and water suspensions (*ca.* 15%, Figure 2c,d). In contrast, the decrease of the integrated area of the induced-electric dipole $^5D_0 \rightarrow {}^7F_2$ Eu^{3+} transition is much larger for suspensions (25%) than for powders (10%), due to the hypersensitivity of this transition to changes in the neighborhood (*e.g.*, in the surrounding medium polarizability). The areas of the $^5D_0 \rightarrow {}^7F_2$ and $^5D_4 \rightarrow {}^7F_5$ lines define the ratiometric thermometric parameter Δ (eq 3) allowing the measurement of the temperature from the emission spectra.

$$\Delta = \frac{I_{Tb}}{I_{Eu}} \quad (3)$$

Although some other empirical definitions of the Δ thermometric parameter are possible,[4,15] an integrated intensity ratio of two emissions is commonly used in ratiometric luminescence temperature sensing. Moreover, this parameter has the distinct advantage of being independent of the particles concentration in the media. The dependence of Δ with temperature provides a calibration curve for the thermometers. Figure 3 shows the calibration curves of **1** in the solid form and in an aqueous suspension, indicating that these materials are luminescent thermometers operative in the 290−320 K range. Upon cycling the temperature, no significant hysteresis is observed, as the Δ parameters measured for different cycles are the same, within experimental error. For simplicity, to have a calibration curve with a thermometric parameter in the range *ca.* 0.9−1.0, the Δ values were normalized to the 303 K value (the lowest common temperature of all cycles). Moreover, the sensitivity (eq 4) may be used as a figure of merit to compare the performance of the luminescent thermometers based on **1** and the performance of other systems reported in the literature.[1]

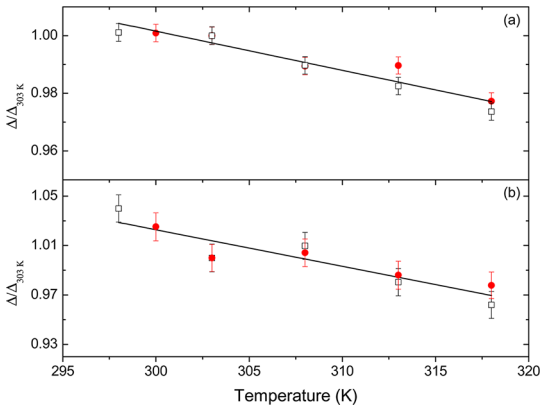

Figure 3. Calibration curves of 1 in (a) solid state and (b) aqueous suspension (0.36 g·L^{-1}) in the range 290−320 K; black squares and red circles represent the first and second heating cycles, respectively. The solid lines are the linear fits $\Delta/\Delta_{303\ K} = 1.41-0.00136T$ ($r^2 > 0.91$) and $\Delta/\Delta_{303\ K} = 1.91-0.00296T$ ($r^2 > 0.81$) for 1 in the solid state and aqueous suspension, respectively. The error bars result from the propagation of the errors (≤1%) in the determination of the $^5D_4 \rightarrow {}^7F_5$ and $^5D_0 \rightarrow {}^7F_2$ transitions areas.

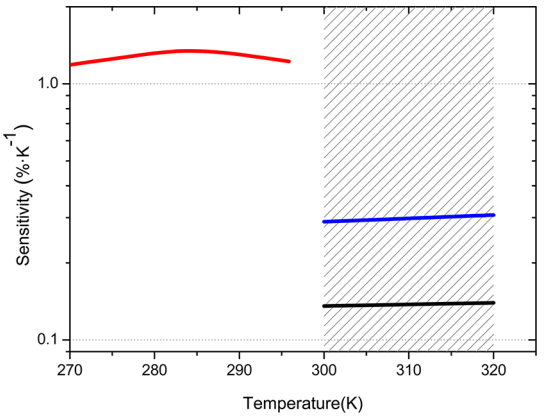

Figure 4. Relative sensitivity of the thermometers 1, in solid state (black) and aqueous suspension (blue), and $(Eu_{0.0069}Tb_{0.9931})_2(DMBDC)_3\ (H_2O)_4\cdot DMF\cdot H_2O$[13] (red). The physiological temperature range is shadowed.

$$S = \frac{\partial\Delta/\partial T}{\Delta} \qquad (4)$$

The sensitivity of **1** (both for water suspension and solid) is almost constant between 298 and 320 K with maximum values of 0.31%·K^{-1} (water suspension) and 0.14%·K^{-1} (solid) at 318 K (Figure 4). The higher sensitivity of the water suspension is due to the large variation of the $^5D_0 \rightarrow {}^7F_2$ integrated area, as discussed above. This is the first Ln-MOF thermometer sensitive in the physiological temperature range. Cui *et al.* reported for $(Eu_xTb_{1-x})_2(DMBDC)_3(H_2O)_4\cdot DMF\cdot H_2O$ micrometer-size particles a maximum sensitivity of 1.3%·K^{-1} at 284 K[13] using the same thermometric parameter presented in eq 3. The work of this group is a significant step forward in cryogenic-temperature sensors due to the excellent linear correlation between the temperature and luminescence intensity ratio from 50 to 200 K; the thermometer is, however, not operative in the physiological temperature range.

CONCLUSIONS

In summary, the potential application of nanorods of $Tb_{0.99}Eu_{0.01}(BDC)_{1.5}(H_2O)_2$ as ratiometric nanothermometers operating in aqueous suspension in the physiological-temperature range was evaluated. A microemulsion method was used to prepare the Tb^{3+}/Eu^{3+} co-doped MOF nanoparticles and their photoluminescence properties studied from 298 to 318 K. The temperature-dependence of the $^5D_0 \rightarrow {}^7F_2$ (Eu^3) and $^5D_4 \rightarrow {}^7F_5$ (Tb^{3+}) transitions was used to define the ratiometric thermometric parameter. Aqueous suspensions of those nanoparticles display an excellent performance as ratiometric luminescent nanothermometers, emission quantum yield of 0.23 ± 0.02 (excitation at 320 nm) and relative sensitivity of 0.37%·K^{-1} at 318 K, pointing out the possibility of using nanoMOFS to measure physiological temperatures in biological applications.

METHODS

Synthesis. $Tb_{0.99}Eu_{0.01}(BDC)_{1.5}(H_2O)_2$ and $Tb(BDC)_{1.5}(H_2O)_2$ nanorods were prepared according to the literature.[31,32] Typically, two $W = 5$ microemulsions were formed by addition of 0.1 M aqueous benzenedicarboxylate disodium salt (112×10^{-6} L) and 0.1 M aqueous $TbCl_3/EuCl_3$ with a 99:1 molar ratio or 0.1 M $TbCl_3$ solution (112×10^{-6} L) to two separate 0.05 M CTAB/1-hexanol/isooctane mixtures (25×10^{-3} L each). The molar ratio for the oil mixture was 1:14:110, respectively. The separate microemulsions were stirred vigorously for 10 min at room temperature after which they were combined. The resultant 50×10^{-3} L microemulsion was stirred vigorously for an additional 2.5 h at room temperature. The nanoparticles were isolated by centrifugation at 6000 rpm for 10 min. After removal of the supernatant, the particles were washed using sonication in ethanol. The ethanol suspension was then centrifuged again for 10 min at 6000 rpm to recover the nanoparticles. This procedure was repeated twice. The solid obtained was dried for one night in an oven at 40 °C. To optimize the emission properties for thermometry, sample with Tb:Eu doping molar ratios from 90:10 to 99:1 were prepared. The latter was used in the studies reported here.

Photoluminescence Measurements. Photoluminescence spectra were recorded with a modular double grating excitation spectrofluorimeter with a TRIAX 320 emission monochromator (Fluorolog-3, Horiba Scientific) coupled to a R928 Hamamatsu photomultiplier, using a front face acquisition mode. The excitation source was a 450 W Xe arc lamp. The emission spectra were corrected for detection and optical spectral response of the spectrofluorimeter and the excitation spectra were corrected for the spectral distribution of the lamp intensity using a photodiode reference detector. The temperature was cycled three times in the 290−320 K, and the emission and excitation spectra were recorded at equal time intervals when the temperature increases. The second and third cycles were used to calibrate the nanothermometers. The temperature was varied using a IES-RD31 controller and a Kapton thermofoil heater from

Minco mounted on a Cu holder and monitored using a thermocouple thermometer Barnant 100 (model 600-2820) with a resolution of 0.1 °C. The emission decay curves were measured with the setup described for the luminescence spectra using a pulsed Xe−Hg lamp (6×10^{-6} s pulse at half width and $(20-30) \times 10^{-6}$ s tail).

Absolute Emission Quantum Yields. The absolute emission quantum yields were measured at room temperature using a quantum yield measurement system C9920-02 from Hamamatsu with a 150 W xenon lamp coupled to a monochromator for wavelength discrimination, an integrating sphere as sample chamber and a multi channel analyzer for signal detection. Three measurements were made for each sample so that the average value is reported. The method is accurate to within 10%.

Conflict of Interest: The authors declare no competing financial interest.

Supporting Information Available: Experimental details on $Tb_{0.99}Eu_{0.01}(BDC)_{1.5}(H_2O)_2$ synthesis and characterization (X-ray powder diffraction, excitation and emission spectra, emission decay curves and lifetime values). This material is available free of charge *via* the Internet at http://pubs.acs.org.

Acknowledgment. We thank COMPETE and FEDER programs and Fundação para a Ciência e a Tecnologia (FCT) (PEst-C/CTM/LA0011/2013) for funding and project REDE/1509/RME/2005 for the access of TEM. C.D.S.B. (SFRH/BPD/89003/2012) thanks FCT for a post-doctoral grant.

REFERENCES AND NOTES

1. Brites, C. D. S.; Lima, P. P.; Silva, N. J. O.; Millán, A.; Amaral, V. S.; Palacio, F.; Carlos, L. D. Thermometry at the Nanoscale. *Nanoscale* **2012**, *4*, 4799–829.
2. Fischer, L. H.; Harms, G. S.; Wolfbeis, O. S. Upconverting Nanoparticles for Nanoscale Thermometry. *Angew. Chem., Int. Ed.* **2011**, *50*, 4546–4551.
3. Jaque, D.; Vetrone, F. Luminescence Nanothermometry. *Nanoscale* **2012**, *4*, 4301–4326.
4. Brites, C. D. S.; Lima, P. P.; Silva, N. J. O.; Millán, A.; Amaral, V. S.; Palacio, F.; Carlos, L. D. A Luminescent Molecular Thermometer for Long-Term Absolute Temperature Measurements at the Nanoscale. *Adv. Mater.* **2010**, *22*, 4499–4504.
5. Peng, H. S.; Huang, S. H.; Wolfbeis, O. S. Ratiometric Fluorescent Nanoparticles for Sensing Temperature. *J. Nanopart. Res.* **2010**, *12*, 2729–2733.
6. Peng, H. S.; Stich, M. I. J.; Yu, J. B.; Sun, L. N.; Fischer, L. H.; Wolfbeis, O. S. Luminescent Europium(III) Nanoparticles for Sensing and Imaging of Temperature in the Physiological Range. *Adv. Mater.* **2010**, *22*, 716–719.
7. Vetrone, F.; Naccache, R.; Zamarron, A.; de la Fuente, A. J.; Sanz-Rodriguez, F.; Maestro, L. M.; Rodriguez, E. M.; Jaque, D.; Solé, J. G.; Capobianco, J. A. Temperature Sensing using Fluorescent Nanothermometers. *ACS Nano* **2010**, *4*, 3254–3258.
8. Saïdi, E.; Samson, B.; Aigouy, L.; Volz, S.; Löw, P.; Bergaud, C.; Mortier, M. Scanning Thermal Imaging by Near-Field Fluorescence Spectroscopy. *Nanotechnology* **2009**, *20*, 115703–11.
9. Singh, S. K.; Kumar, K.; Rai, S. B. Multifunctional Er^{3+}-Yb^{3+} Codoped Gd_2O_3 Nanocrystalline Phosphor Synthesized Through Optimized Combustion Route. *Appl. Phys. B: Lasers Opt.* **2009**, *94*, 165–173.
10. Dong, N. N.; Pedroni, M.; Piccinelli, F.; Conti, G.; Sbarbati, A.; Ramírez-Hernández, J. E.; Maestro, L. M.; Iglesias-de la Cruz, M. C.; Sanz-Rodriguez, F.; Juarranz, A.; *et al.* NIR-to-NIR Two-Photon Excited CaF_2:Tm^{3+},Yb^{3+} Nanoparticles: Multifunctional Nanoprobes for Highly Penetrating Fluorescence Bio-Imaging. *ACS Nano* **2011**, *5*, 8665–71.
11. Alencar, M. A. R. C.; Maciel, G. S.; de Araújo, C. B.; Patra, A. Er^{3+}-Doped $BaTiO_3$ Nanocrystals for Thermometry: Influence of Nanoenvironment on the Sensitivity of a Fluorescence Based Temperature Sensor. *Appl. Phys. Lett.* **2004**, *84*, 4753–4755.
12. Rocha, U.; Jacinto, C.; Silva, W. F.; Guedes, I.; Benayas, A.; Maestro, L. M.; Elias, M. A.; Bovero, E.; van Veggel, F. C. J. M.; Solé, J. G.; *et al.* Subtissue Thermal Sensing Based on Neodymium-Doped LaF_3 Nanoparticles. *ACS Nano* **2013**, *7*, 1188–1199.
13. Cui, Y. J.; Xu, H.; Yue, Y. F.; Guo, Z. Y.; Yu, J. C.; Chen, Z. X.; Gao, J. K.; Yang, Y.; Qian, G. D.; Chen, B. L. A Luminescent Mixed-Lanthanide Metal-Organic Framework Thermometer. *J. Am. Chem. Soc.* **2012**, *134*, 3979–3982.
14. Brites, C. D. S.; Lima, P. P.; Silva, N. J. O.; Millán, A.; Amaral, V. S.; Palacio, F.; Carlos, L. D. Ratiometric Highly Sensitive Luminescent Nanothermometers Working in the Room Temperature Range. Applications to Heat Propagation in Nanofluids. *Nanoscale* **2013**, 10.1039/C3NR02335D.
15. Brites, C. D. S.; Lima, P. P.; Silva, N. J. O.; Millán, A.; Amaral, V. S.; Palacio, F.; Carlos, L. D. Thermometry at the Nanoscale Using Lanthanide-Containing Organic-Inorganic Hybrid Materials. *J. Lumin.* **2013**, *133*, 230–232.
16. Allendorf, M. D.; Bauer, C. A.; Bhakta, R. K.; Houk, R. J. T. Luminescent Metal-Organic Frameworks. *Chem. Soc. Rev.* **2009**, *38*, 1330–1352.
17. Rocha, J.; Carlos, L. D.; Paz, F. A. A.; Ananias, D. Luminescent Multifunctional Lanthanides-Based Metal-Organic Frameworks. *Chem. Soc. Rev.* **2011**, *40*, 926–940.
18. Cui, Y. J.; Yue, Y. F.; Qian, G. D.; Chen, B. L. Luminescent Functional Metal-Organic Frameworks. *Chem. Rev.* **2012**, *112*, 1126–1162.
19. Rieter, W. J.; Pott, K. M.; Taylor, K. M. L.; Lin, W. B. Nanoscale Coordination Polymers for Platinum-Based Anticancer Drug Delivery. *J. Am. Chem. Soc.* **2008**, *130*, 11584–11585.
20. Xu, H.; Liu, F.; Cui, Y. J.; Chen, B. L.; Qian, G. D. A Luminescent Nanoscale Metal-Organic Framework for Sensing of Nitroaromatic Explosives. *Chem. Commun.* **2011**, *47*, 3153–3155.
21. Della Rocca, J.; Liu, D. M.; Lin, W. B. Nanoscale Metal-Organic Frameworks for Biomedical Imaging and Drug Delivery. *Acc. Chem. Res.* **2011**, *44*, 957–968.
22. Yang, W. T.; Feng, J.; Zhang, H. J. Facile and Rapid Fabrication of Nanostructured Lanthanide Coordination Polymers as Selective Luminescent Probes in Aqueous Solution. *J. Mater. Chem.* **2012**, *22*, 6819–6823.
23. Chen, B. L.; Xiang, S. C.; Qian, G. D. Metal-Organic Frameworks with Functional Pores for Recognition of Small Molecules. *Acc. Chem. Res.* **2010**, *43*, 1115–1124.
24. Harbuzaru, B. V.; Corma, A.; Rey, F.; Atienzar, P.; Jorda, J. L.; Garcia, H.; Ananias, D.; Carlos, L. D.; Rocha, J. Metal-Organic Nanoporous Structures with Anisotropic Photoluminescence and Magnetic Properties and Their Use as Sensors. *Angew. Chem., Int. Ed.* **2008**, *47*, 1080–1083.
25. Lan, A. J.; Li, K. H.; Wu, H. H.; Olson, D. H.; Emge, T. J.; Ki, W.; Hong, M. C.; Li, J. A Luminescent Microporous Metal-Organic Framework for the Fast and Reversible Detection of High Explosives. *Angew. Chem., Int. Ed.* **2009**, *48*, 2334–2338.
26. White, K. A.; Chengelis, D. A.; Gogick, K. A.; Stehman, J.; Rosi, N. L.; Petoud, S. Near-Infrared Luminescent Lanthanide MOF Barcodes. *J. Am. Chem. Soc.* **2009**, *131*, 18069–18071.
27. Lin, W. B.; Rieter, W. J.; Taylor, K. M. L. Modular Synthesis of Functional Nanoscale Coordination Polymers. *Angew. Chem., Int. Ed.* **2009**, *48*, 650–658.
28. Harbuzaru, B. V.; Corma, A.; Rey, F.; Jorda, J. L.; Ananias, D.; Carlos, L. D.; Rocha, J. A Miniaturized Linear pH Sensor Based on a Highly Photoluminescent Self-Assembled Europium(III) Metal-Organic Framework. *Angew. Chem., Int. Ed.* **2009**, *48*, 6476–6479.
29. Liu, K.; You, H. P.; Zheng, Y. H.; Jia, G.; Song, Y. H.; Huang, Y. J.; Yang, M.; Jia, J. J.; Guo, N.; Zhang, H. J. Facile and Rapid Fabrication of Metal-Organic Framework Nanobelts and Color-Tunable Photoluminescence Properties. *J. Mater. Chem.* **2010**, *20*, 3272–3279.
30. Weber, I. T.; de Melo, A. J. G.; Lucena, M. A. D.; Rodrigues, M. O.; Alves, S. High Photoluminescent Metal-Organic Frameworks as Optical Markers for the Identification of Gunshot Residues. *Anal. Chem.* **2011**, *83*, 4720–4723.

31. Rieter, W. J.; Taylor, K. M. L.; An, H. Y.; Lin, W. L.; Lin, W. B. Nanoscale Metal-Organic Frameworks as Potential Multimodal Contrast Enhancing Agents. *J. Am. Chem. Soc.* **2006**, *128*, 9024–9025.
32. Taylor, K. M. L.; Jin, A.; Lin, W. B. Surfactant-Assisted Synthesis of Nanoscale Gadolinium Metal-Organic Frameworks for Potential Multimodal Imaging. *Angew. Chem., Int. Ed.* **2008**, *47*, 7722–7725.
33. Reineke, T. M.; Eddaoudi, M.; Fehr, M.; Kelley, D.; Yaghi, O. M. From Condensed Lanthanide Coordination Solids to Microporous Frameworks Having Accessible Metal Sites. *J. Am. Chem. Soc.* **1999**, *121*, 1651–1657.
34. Ferreira, R. A. S.; Nolasco, M.; Roma, A. C.; Longo, R. L.; Malta, O. L.; Carlos, L. D. Dependence of the Lifetime Upon the Excitation Energy and Intramolecular Energy Transfer Rates: The $^5D_0$ Eu(III) Emission Case. *Chem.—Eur. J.* **2012**, *18*, 12130–12139.
35. Reisfeld, R.; Jørgenson, C. K. Excited State Phenomena *in Vitreous* Materials. In *Handbook on the Physics and Chemistry of Rare Earths*; Gschneider, K. A. J., Eyring, L., Eds.; Elsevier Science Publishers: Amsterdam, 1987; Vol. 9, pp 1−90.
36. Ananias, D.; Kostova, M.; Paz, F. A. A.; Ferreira, A.; Carlos, L. D.; Klinowski, J.; Rocha, J. Photoluminescent Layered Lanthanide Silicates. *J. Am. Chem. Soc.* **2004**, *126*, 10410–10417.
37. Daiguebonne, C.; Kerbellec, N.; Guillou, O.; Bünzli, J. C.; Gumy, F.; Catala, L.; Mallah, T.; Audebrand, N.; Gerault, Y.; Bernot, K.; *et al.* Structural and Luminescent Properties of Micro- and Nanosized Particles of Lanthanide Terephthalate Coordination Polymers. *Inorg. Chem.* **2008**, *47*, 3700–3708.
38. de Lill, D. T.; de Bettencourt-Dias, A.; Cahill, C. L. Exploring Lanthanide Luminescence in Metal-Organic Frameworks: Synthesis, Structure, and Guest-Sensitized Luminescence of a Mixed Europium/Terbium-Adipate Framework and a Terbium-Adipate Framework. *Inorg. Chem.* **2007**, *46*, 3960–3965.